PERGAMON

International Journal of Solids and Structures 39 (2002) 4543–4565

INTERNATIONAL JOURNAL OF SOLIDS and STRUCTURES

www.elsevier.com/locate/ijsolstr

Developments of some explicit formulas useful to describe elastic stress fields ahead of notches in plates

S. Filippi [a], P. Lazzarin [b,*], R. Tovo [c]

[a] *Department of Mechanical Engineering, University of Padova, Via Venezia 1, 35131 Padova, Italy*
[b] *Department of Management and Engineering, University of Padova, Stradella S. Nicola 3, 36100 Vicenza, Italy*
[c] *Department of Engineering, University of Ferrara, Via Saragat 1, 44100 Ferrara, Italy*

Received 15 May 2001; received in revised form 8 May 2002

Abstract

The paper deals with the evaluation of linear elastic stress fields in the neighbourhood of U- and V-shaped notches in plane plates. The main aim is to improve the accuracy of an approximate solution already proposed in the literature by changing the polynomial arrangement of complex potential functions and properly adapting the boundary conditions. In some special cases, the solution matches Williams, Westergaard–Irwin and Creager–Paris' equations universally used in the case of sharp corners, cracks, and blunt cracks, respectively. In the presence of notches with a tip radius different from zero and a large opening angle, the equations obtained are compared with finite element results, showing a very good agreement. Due to their reduced complexity, such equations turn out to be particularly useful when applied to rounded V-notches as well as welded-like geometries under mixed loading conditions. Finally, some limits of the solution when applied to the notch free edges are highlighted.

Keywords: V-notch; Elasticity; Complex potential function; Stress concentration factor; Notch stress intensity factor

1. Introduction

The knowledge of the whole stress–strain field close to the notch tip, and not only the peak stress value, is particularly useful in mechanical design since it can help to evaluate properly the geometrical effects on the strength of components, principally when their fatigue behaviour is concerned.

For the linear elastic analysis of plane cases, conventional approaches have been soundly established since Kolosov (1909) and Muskhelishvili (1953), and Neuber (1958), who used complex potential functions and bi-harmonic potential functions, respectively. As far as sharp notches are concerned, main contributions have been the crack solution due to Westergaard (1939) and Irwin (1957) and the sharp V-shaped notch solution due to Williams (1952). Blunt cracks, i.e. slim parabolic notches, have been dealt with by Creager and Paris (1967), and then by Glinka (1985) who was able to give a closed-form expression to the

* Corresponding author. Tel.: +39-444-998-711/780; fax: +39-444-998-888.
E-mail address: plazzarin@gest.unipd.it (P. Lazzarin).

0020-7683/02/$ - see front matter
PII: S0020-7683(02)00342-6

generalised stress intensity factors (SIF) in Creager–Paris' equations. In the close neighbourhood of the notch tip, where stress distributions mainly depend on the notch tip radius, such equations continue to be a very powerful tool.

More recently, Lazzarin and Tovo (1996) gave a solution dealing with sharp and rounded V-notches, the crack and the blunt crack being particular cases of the unifying solution capable of addressing any combination of notch tip radius and opening angle. Afterwards, Lazzarin et al. (1998) extended that approach in order to take into account also the influence of plate finite size on the stress fields. Other formulations already reported in the literature (Glinka and Newport, 1987; Xu et al., 1995; Kujawski and Shin, 1997), and focusing mainly on the maximum principal stress distribution along the notch bisector, have already been discussed (Lazzarin et al., 1998; Atzori et al., 1997).

As already stated by the authors, the approximated formulas provided by Lazzarin and Tovo (1996) showed a lack of accuracy in describing the stress field due to rounded V-shaped notches with a large opening angle. However, since such a type of geometry had not been previously described by any other analytical solution, the progress given by that proposal appeared to be substantial.

This paper aims to improve greatly the accuracy of the past solution and to extend its range of applicability, avoiding excessive complications in the stress field expressions. By so doing, the new expressions are considered feasible for cases of engineering interests.

Finally, the paper aims to clarify the limits of applicability and the degree of accuracy of stress expressions when applied to notches under mixed loading conditions, with particular emphasis on the predictions valid for notch free edges.

2. Previous solution

The case investigated in the present stress analysis is the round open notch sketched in Fig. 1 together with the frame of reference and the stress component definitions.

The old solution (Lazzarin and Tovo, 1996) adopted, according to Kolosoff–Muskhelishvili's method, two analytical potential functions:

$$\varphi(z) = az^{\lambda}, \qquad \psi(z) = bz^{\lambda} + cz^{\mu} \tag{1}$$

where coefficients a, b and c were complex, exponents λ and μ were real, with $\lambda > 0$ and $\lambda > \mu$. When c is null, the approach matches Williams' solution (Carpenter, 1984a).

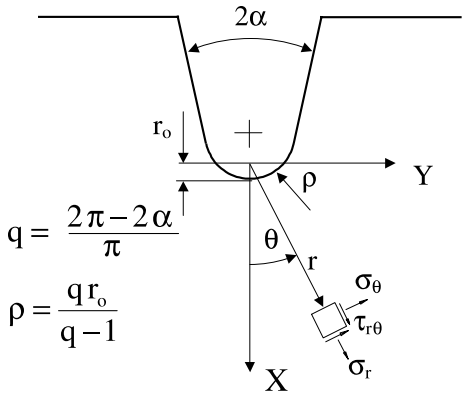

Fig. 1. Coordinate system and symbols used for the stress field components.

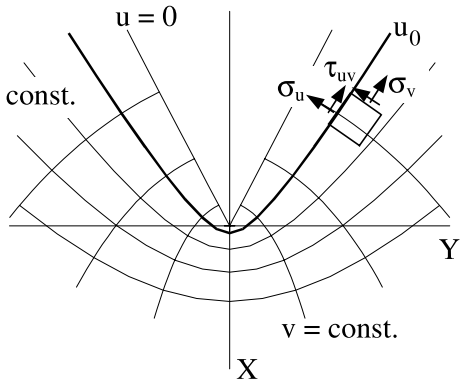

Fig. 2. Auxiliary system of curvilinear coordinates (u, v).

The boundary conditions were imposed on an auxiliary system of curvilinear coordinates u and v, the relation with the Cartesian coordinates x–y being as follows (Fig. 2):

$$x + \mathrm{i}y = (u + \mathrm{i}v)^q \tag{2}$$

In Eq. (2) "q" is a real coefficient ranging from 1 (flat edge) to 2 (crack). The curve defined by $u = 0$ describes an angle equal to 2α, related to "q" by the expression

$$2\alpha = \pi(2 - q) \tag{3}$$

The chosen free edge approximating the investigated geometry is the curve $u = u_0$ and its notch tip radius is related to u_0 by means of

$$\rho = \frac{q u_0^q}{q - 1} = \frac{q r_0}{q - 1} \tag{4}$$

The free edge condition requires that σ_u and τ_{uv} stress components should be zero along the whole edge, that is

$$(\sigma_u)_{u=u_0} = 0, \qquad (\tau_{uv})_{u=u_0} = 0 \tag{5}$$

Due to the reduced number of free parameters and the particular choice of potential functions given by Eq. (1), the boundary conditions could be completely satisfied only when the null notch tip radius is null, i.e. in the corner case (Williams, 1952). Elsewhere the boundary conditions were simplified by ensuring that Eq. (5) was satisfied in the close neighbourhood of the notch tip and far from it. The resulting conditions were

$$(\sigma_u)_{\substack{u=u_0 \\ v=0}} = (\sigma_r)_{\substack{r=r_0 \\ \theta=0}} = 0, \qquad (\tau_{uv})_{\substack{u=u_0 \\ v=0}} = (\tau_{r\theta})_{\substack{r=r_0 \\ \theta=0}} = 0 \tag{6a,b}$$

$$\left(\frac{\partial \sigma_u}{\partial v}\right)_{\substack{u=u_0 \\ v=0}} = \left(\frac{\partial \sigma_r}{\partial \theta} - \frac{2}{q}\tau_{r\theta}\right)_{\substack{r=r_0 \\ \theta=0}} = 0, \qquad \left(\frac{\partial \tau_{uv}}{\partial v}\right)_{\substack{u=u_0 \\ v=0}} = \left(\frac{\partial \tau_{r\theta}}{\partial \theta} - \frac{1}{q}\sigma_\theta\right)_{\substack{r=r_0 \\ \theta=0}} = 0 \tag{7a,b}$$

$$(\sigma_u)_{\substack{u=u_0 \\ v \gg v_0}} = 0 \Rightarrow \lim_{\substack{r\to\infty \\ \theta\to\pm q\pi/2}} \left(r^{1-\lambda}\sigma_\theta\right) = 0, \qquad (\tau_{uv})_{\substack{u=u_0 \\ v \gg v_0}} = 0 \Rightarrow \lim_{\substack{r\to\infty \\ \theta\to\pm q\pi/2}} \left(r^{1-\lambda}\tau_{r\theta}\right) = 0 \tag{8a,b}$$

While Eqs. (6a,b) and (7a,b) are obvious, Eq. (8a,b) needs some clarification:

- At a convenient distance from the notch tip ($r = \bar{r}$) the z^{μ} term is negligible with respect to the z^{λ} term. Consequently, Eq. (8a,b) can be written involving only the λ related stress components.
- There exists also a distance ($r = \bar{\bar{r}}$) at which the $\theta = \pm q\pi/2$ straight lines departing from the origin of the coordinate system are very close to the real boundary and, therefore, σ_θ and $\tau_{r\theta}$ coincide with σ_u and τ_{uv}, respectively.
- Since, in general, $\bar{r}$ and $\bar{\bar{r}}$ cannot be "a priori" defined exactly, the radial distance r is set equal to infinite in Eq. (8a,b). It turns out that az^{λ} and bz^{λ} terms are zero for $r \to \infty$ and $\theta = \pm q\pi/2$.

In the neighbourhood of the notch tip, the profile of a real V-shaped notch is different from the theoretical profile given by Eq. (2); however, at the notch tip, both profiles present the same radius of curvature ρ. When finite boundaries (or finite geometries) are considered, the analytical equations, corresponding to the infinite domain, can be efficiently used only when the notch tip radius is small with respect to the notch depth and the two sides of the notch are represented by straight lines.

It is well known that the stress distributions in the neighbourhood of the tip depend mainly on the notch tip radius (Xu et al., 1995). The dimension of such a zone was demonstrated to be 0.4 ρ (Atzori et al., 2001) in plates weakened by semicircular, semi-elliptic and V-shaped notches (with an opening angle ranging from 0° to 135°), all subjected to mode I load conditions. Outside this region, the influence of the opening angle becomes evident, and the stress fields induced by rounded V-notches approached closely those of sharp V-notches (Atzori et al., 2001). This means that the effect of the notch tip radius and the opening angle can be seen as "independent".

The results obtained by Lazzarin and Tovo (1996) provided the main trend of stress fields for very different geometries. However, as already highlighted by the authors, some disagreements were found between theoretical and numerical results for rounded V-shaped notches, in particular in the zone where stresses become sensitive to both the notch tip radius and also to the notch opening angle. In such a zone, the maximum principal stress exhibits a linear trend along the notch bisector when plotted in a double logarithmic diagram.

As an example, the principal stress along the "X" direction of a 135° V-shaped notch is shown in Fig. 3. It is evident that, at distances from the tip comparable with the notch radius, the analytical curve and the

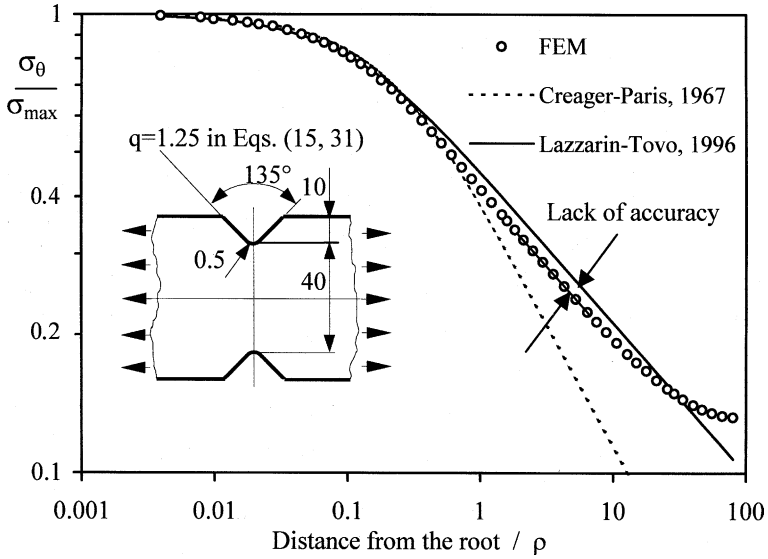

Fig. 3. A comparison between numerical and analytical results along the notch bisector.

numerical values (coincident at the tip) have the same slope and that such a slope depends on the opening angle. On the other hand, there is a small gap between the two estimations and this inconsistency obviously affects the accuracy of the formulation. Fig. 3 also shows that it is not possible to neglect the influence of the notch opening angle ahead of the notch, as could be done by improperly using Creager–Paris' equations.

3. An improved solution for stress distributions

With the aim of improving the accuracy of the analytical solution, the previous approach has been modified. The lack of correctness seems to arise close to the notch tip, where terms with the exponent "μ" give a significant contribution. The basic idea is to achieve greater precision by adding more factors, and then more flexibility, to the part of the equations with exponent "μ".

By adding a term to the first of the two analytical functions, they become

$$\varphi(z) = az^{\lambda} + dz^{\mu}, \qquad \psi(z) = bz^{\lambda} + cz^{\mu} \tag{9}$$

Then, the general expressions of stress components turn out to be:

$$\begin{aligned}\sigma_\theta = {} & \lambda r^{\lambda-1}[a_1(1+\lambda)\cos(1-\lambda)\theta + b_1\cos(1+\lambda)\theta + a_2(1+\lambda)\sin(1-\lambda)\theta - b_2\sin(1+\lambda)\theta] \\ & + \mu r^{\mu-1}[d_1(1+\mu)\cos(1-\mu)\theta + c_1\cos(1+\mu)\theta + d_2(1+\mu)\sin(1-\mu)\theta - c_2\sin(1+\mu)\theta]\end{aligned} \tag{10}$$

$$\begin{aligned}\sigma_r = {} & \lambda r^{\lambda-1}[a_1(3-\lambda)\cos(1-\lambda)\theta - b_1\cos(1+\lambda)\theta + a_2(3-\lambda)\sin(1-\lambda)\theta + b_2\sin(1+\lambda)\theta] \\ & + \mu r^{\mu-1}[d_1(3-\mu)\cos(1-\mu)\theta - c_1\cos(1+\mu)\theta + d_2(3-\mu)\sin(1-\mu)\theta + c_2\sin(1+\mu)\theta]\end{aligned} \tag{11}$$

$$\begin{aligned}\tau_{r\theta} = {} & \lambda r^{\lambda-1}[a_1(1-\lambda)\sin(1-\lambda)\theta + b_1\sin(1+\lambda)\theta - a_2(1-\lambda)\cos(1-\lambda)\theta + b_2\cos(1+\lambda)\theta] \\ & + \mu r^{\mu-1}[d_1(1-\mu)\sin(1-\mu)\theta + c_1\sin(1+\mu)\theta - d_2(1-\mu)\cos(1-\mu)\theta + c_2\cos(1+\mu)\theta]\end{aligned} \tag{12}$$

where indexes 1 and 2 denote the real and imaginary part of constants, respectively.

Note that, as in the previous solutions, the stress field distribution will turn out to be singular at the point $z = 0$; however, this point is outside the bounds of the physical domain, so that we can completely disregard the singularity.

It is noteworthy that this choice of a potential function is actually obtained by doubling the one already suggested by Williams (1952). Moreover, the stress functions chosen are linearly related to the added constant "d", so that the equations have not been made substantially more complex.

Each parameter must be determined by imposing the boundary conditions, which are those given by Eq. (5). Even in this case they cannot be satisfied along the whole free edge and must be somehow simplified.

Being $(-\theta/q)$ the angle included between the principal directions of the polar and the curvilinear systems, the components of the stress field in the (u, v) curvilinear system can be now derived from (10)–(12) by imposing the local rotation of the reference system previously defined (Lazzarin and Tovo, 1996):

$$\begin{aligned}\sigma_u &= \frac{1}{2}(\sigma_r + \sigma_\theta) + \frac{1}{2}(\sigma_r - \sigma_\theta)\cos\frac{2\theta}{q} - \tau_{r\theta}\sin\frac{2\theta}{q} \\ \sigma_v &= \frac{1}{2}(\sigma_r + \sigma_\theta) - \frac{1}{2}(\sigma_r - \sigma_\theta)\cos\frac{2\theta}{q} + \tau_{r\theta}\sin\frac{2\theta}{q} \\ \tau_{uv} &= \frac{1}{2}(\sigma_r - \sigma_\theta)\sin\frac{2\theta}{q} + \tau_{r\theta}\cos\frac{2\theta}{q}\end{aligned} \tag{13}$$

Eq. (8a,b) in σ_u and Eq. (8a,b) in τ_{uv} give the same homogeneous system conditions proposed by Williams (1952) for V-crack.

$$\begin{bmatrix} (1+\lambda)\cos\left[(1-\lambda)q\frac{\pi}{2}\right]\cos\left[(1+\lambda)q\frac{\pi}{2}\right] & 0 \\ (1-\lambda)\sin\left[(1-\lambda)q\frac{\pi}{2}\right]\sin\left[(1+\lambda)q\frac{\pi}{2}\right] & \\ 0 & (1+\lambda)\sin\left[(1-\lambda)q\frac{\pi}{2}\right]-\sin\left[(1+\lambda)q\frac{\pi}{2}\right] \\ & (1-\lambda)\cos\left[(1-\lambda)q\frac{\pi}{2}\right]-\cos\left[(1+\lambda)q\frac{\pi}{2}\right] \end{bmatrix} \begin{Bmatrix} a_1 \\ b_1 \\ a_2 \\ b_2 \end{Bmatrix} = \begin{Bmatrix} 0 \\ 0 \\ 0 \\ 0 \end{Bmatrix} \tag{14}$$

Solutions are not trivial only if the two uncoupled determinants are equal to zero. This leads to the following equations for λ:

$$\sin(\lambda_1 q\pi) + \lambda_1 \sin(\pi q) = 0 \qquad \text{(Mode I)} \tag{15}$$

$$\sin(\lambda_2 q\pi) - \lambda_2 \sin(\pi q) = 0 \qquad \text{(Mode II)} \tag{16}$$

In general, Eqs. (15) and (16) can give n-solutions or eigenvalues. The problem being linear, the general solution can be given as a linear combination of all particular solutions (Williams, 1957; Carpenter, 1984b, 1985); however, the state of stress and displacement near the corner is dominated by the first eigenvector so that only the eigenvalue with the lowest modulus have been considered in our analyses.

By excluding for the moment the zero opening case, parameters b_1 and b_2 can be given as a function of the undetermined coefficients a_1 and a_2. For the symmetric problem, denoted by index 1, one obtains

$$b_1 = \chi_{b_1}(1-\lambda_1)a_1 \tag{17}$$

where

$$\chi_{b_1} = -\frac{\sin[(1-\lambda_1)q\pi/2]}{\sin[(1+\lambda_1)q\pi/2]} \tag{18}$$

The skew-symmetric problem results in:

$$b_2 = -\chi_{b_2}(1+\lambda_2)a_2 \tag{19}$$

where

$$\chi_{b_2} = -\frac{\sin[(1-\lambda_2)q\pi/2]}{\sin[(1+\lambda_2)q\pi/2]} \tag{20}$$

For the zero opening or crack problem, all the terms of the coefficient matrix of (14) are zero for those eigenvalues which make the determinant zero and there are two coefficient associated with each eigenvector (Carpenter, 1984a,b). However, the first and the second eigenvalues are equal and the related eigenvector is associated to two coefficients related to mode I and II fracture (as clearly stated by Carpenter (1985)). Hence, also in this case, the first symmetric and the first skew-symmetric eigenvector are defined except for a single constant.

Dealing with the remaining constants and parameter evaluation, it is necessary to note that, compared with the conditions imposed in (Lazzarin and Tovo, 1996), additional conditions must be used due to the increased number of free parameters. The former condition has to deal with the symmetric part of the problem, the latter with the skew-symmetric one.

It has been chosen to demand the zero traction condition also on the "μ" components far away from the tip. Such a condition has been imposed on σ_u and τ_{uv} stress components in the following way:

$$(\sigma_u)_{\substack{u=u_0,\\ v\ll -v_0}} + (\sigma_u)_{\substack{u=u_0,\\ v\gg v_0}} = 0 \Rightarrow \lim_{\substack{r\to\infty\\ \theta\to -q\pi/2}} (r^{1-\mu}\sigma_\theta) + \lim_{\substack{r\to\infty\\ \theta\to +q\pi/2}} (r^{1-\mu}\sigma_\theta) = 0 \tag{21}$$

$$(\tau_{uv})_{\substack{u=u_0,\\ v\gg v_0}} - (\tau_{uv})_{\substack{u=u_0,\\ v\ll -v_0}} = 0 \Rightarrow \lim_{\substack{r\to\infty\\ \theta\to +q\pi/2}} (r^{1-\mu}\tau_{r\theta}) - \lim_{\substack{r\to\infty\\ \theta\to -q\pi/2}} (r^{1-\mu}\tau_{r\theta}) = 0 \tag{22}$$

Differently from the assumptions given by Eq. (8a,b), which have been used to determine four free parameters for the λ components, in the new solution only two added parameters in the μ components are actually free, i.e. d_1 and d_2. Then, only two additional boundary conditions are required. Hence the "far away" conditions given by Eqs. (21) and (22) on the μ components have to be reduced, in contrast to what has been done with the Eq. (8a,b). Specifically, it has been chosen to force to zero the symmetric part of the tensile stress (that is mainly involved in symmetric loading) in Eq. (21) and only the skew-symmetric part of the shear stress field in Eq. (22). By applying now the stress field expressions (10)–(12) to the free-edge conditions (6a,b), (7a,b), (21) and (22), a new explicit set of equations can be derived.

Consider now the symmetric solution only. By introducing Eqs. (10)–(12) into Eqs. (6a), (7b) and (21) one obtains the parameters μ_1, c_1, d_1

$$\lambda_1 r_0^{\lambda_1-1}\left(3-\lambda_1-\frac{b_1}{a_1}\right) + \mu_1 r_0^{\mu_1-1}\left[(3-\mu_1)\frac{d_1}{a_1}-\frac{c_1}{a_1}\right] = 0 \tag{23}$$

$$\lambda_1 r_0^{\lambda_1-1}\left[(1-\lambda_1)^2+\frac{b_1}{a_1}(1+\lambda_1)\right] + \mu_1 r_0^{\mu_1-1}\left[(1-\mu_1)^2\frac{d_1}{a_1}+\frac{c_1}{a_1}(1+\mu_1)\right] - \frac{1}{q}\lambda_1 r_0^{\lambda_1-1}\left[(1+\lambda_1)+\frac{b_1}{a_1}\right] - \frac{1}{q}\mu_1 r_0^{\mu_1-1}\left[(1+\mu_1)\frac{d_1}{a_1}+\frac{c_1}{a_1}\right] = 0 \tag{24}$$

$$\frac{d_1}{a_1}(1+\mu_1)\cos\left[(1-\mu_1)q\frac{\pi}{2}\right] + \frac{c_1}{a_1}\cos\left[(1+\mu_1)q\frac{\pi}{2}\right] = 0 \tag{25}$$

Note that Eqs. (23)–(25) are linearly dependent on the indexes c_1 and d_1, so they are not significantly more complex than the corresponding equations in the old solution. By using Eqs. (23) and (24), the parameters c_1 and d_1 are obtained as

$$c_1 = \frac{q\lambda_1 r_0^{\lambda_1-\mu_1}}{4\mu_1(q-1)}\chi_{c_1}a_1 \tag{26}$$

$$d_1 = \frac{q\lambda_1 r_0^{\lambda_1-\mu_1}}{4\mu_1(q-1)}\chi_{d_1}a_1 \tag{27}$$

where the auxiliary indexes χ_{c_1}, χ_{d_1} are as follows:

$$\chi_{c_1} = \left[(1-\mu_1)^2-\frac{1}{q}(1+\mu_1)\right]\left[(3-\lambda_1)-\chi_{b_1}(1-\lambda_1)\right] - (3-\mu_1)\varepsilon_1 \tag{28}$$

$$\chi_{d_1} = \left[\frac{1-q(1+\mu_1)}{q}\right]\left[3-\lambda_1-\chi_{b_1}(1-\lambda_1)\right] - \varepsilon_1 \tag{29}$$

being

$$\varepsilon_1 = (1-\lambda_1)^2 + \chi_{b_1}(1-\lambda_1^2) - \frac{1}{q}(1+\lambda_1) - \frac{1}{q}\chi_{b_1}(1-\lambda_1) \tag{30}$$

The exponent μ_1 is given by the implicit solution of the following equation:

$$\left\{\left[\frac{1-q(1+\mu_1)}{q}\right]\left[3-\lambda_1-\chi_{b_1}(1-\lambda_1)\right]-\varepsilon_1\right\}(1+\mu_1)\cos\left[(1-\mu_1)q\frac{\pi}{2}\right]+\left\{\left[(1-\mu_1)^2-\frac{1+\mu_1}{q}\right]\times\left[3-\lambda_1-\chi_{b_1}(1-\lambda_1)\right]-(3-\mu_1)\varepsilon_1\right\}\cos\left[(1+\mu_1)q\frac{\pi}{2}\right]=0 \tag{31}$$

When the notch radius is equal to zero, the distance r_0 is null. Then c_1 and d_1 are also null (see Eqs. (26) and (27)) and the equations for stresses simplify.

The skew-symmetric part of the problem, denoted here by index 2, can be dealt with in an analogous way. By introducing Eqs. (10)–(12) into the boundary conditions Eqs. (6b), (7a) and (22), one obtains

$$\lambda_2 r_0^{\lambda_2-1}\left(-1+\lambda_2+\frac{b_2}{a_2}\right)+\mu_2 r_0^{\mu_2-1}\left[-(1-\mu_2)\frac{d_2}{a_2}+\frac{c_2}{a_2}\right]=0 \tag{32}$$

$$\lambda_2 r_0^{\lambda_2-1}\left[(1-\lambda_2)(3-\lambda_2)+(1+\lambda_2)\frac{b_2}{a_2}\right]+\mu_2 r_0^{\mu_2-1}\left[(1-\mu_2)(3-\mu_2)\frac{d_2}{a_2}+(1+\mu_2)\frac{c_2}{a_2}\right]-\frac{2}{q}\lambda_2 r_0^{\lambda_2-1}\left[-(1-\lambda_2)+\frac{b_2}{a_2}\right]-\frac{2}{q}\mu_2 r_0^{\mu_2-1}\left[-(1-\mu_2)\frac{d_2}{a_2}+\frac{c_2}{a_2}\right]=0 \tag{33}$$

$$-\frac{d_2}{a_2}(1-\mu_2)\cos\left[(1-\mu_2)q\frac{\pi}{2}\right]+\frac{c_2}{a_2}\cos\left[(1+\mu_2)q\frac{\pi}{2}\right]=0 \tag{34}$$

The expressions for c_2 and d_2 are

$$c_2=\frac{\lambda_2 r_0^{\lambda_2-\mu_2}}{4\mu_2(\mu_2-1)}\chi_{c_2}a_2 \tag{35}$$

$$d_2=\frac{\lambda_2 r_0^{\lambda_2-\mu_2}}{4\mu_2(\mu_2-1)}\chi_{d_2}a_2 \tag{36}$$

where the required auxiliary coefficients are

$$\varepsilon_2=(3-\lambda_2)(1-\lambda_2)-\chi_{b_2}(1+\lambda_2)^2+\frac{2}{q}(1-\lambda_2)+\frac{2}{q}\chi_{b_2}(1+\lambda_2) \tag{37}$$

$$\chi_{c_2}=(\mu_2-1)\left[\frac{q(\mu_2-3)-2}{q}\right]\left[(\lambda_2-1)-\chi_{b_2}(1+\lambda_2)\right]+(1-\mu_2)\varepsilon_2 \tag{38}$$

$$\chi_{d_2}=-\left[\frac{q(1+\mu_2)-2}{q}\right]\left[\lambda_2-1-\chi_{b_2}(1+\lambda_2)\right]+\varepsilon_2 \tag{39}$$

The exponent μ_2 is defined by the following implicit equation:

$$\left\{\left[\frac{q(1+\mu_2)-2}{q}\right]\left[\lambda_2-1-\chi_{b_2}(1+\lambda_2)\right]-\varepsilon_2\right\}(1-\mu_2)\cos\left[q\frac{\pi}{2}(1-\mu_2)\right]+\left\{(\mu_2-1)\left[\frac{q(\mu_2-3)-2}{q}\right]\times\left[\lambda_2-1-\chi_{b_2}(1+\lambda_2)\right]+(1-\mu_2)\varepsilon_2\right\}\cos\left[q\frac{\pi}{2}(1+\mu_2)\right]=0 \tag{40}$$

Eqs. (31) and (40) represent a second order eigenvalue problem which is correlated to Williams' solution. When the notch tip radius is null, coefficients c_2 and d_2 are also null since $r_0=0$ and the origin of the coordinate system coincides with the corner apex.

The stress components can be written by separating the contribution due to the symmetric solution (mode I) from that due to the skew-symmetric solution (mode II).

Stresses due to mode I loading conditions are

$$\begin{Bmatrix}\sigma_\theta\\ \sigma_r\\ \tau_{r\theta}\end{Bmatrix} = \lambda_1 r^{\lambda_1-1} a_1 \left[\begin{Bmatrix}(1+\lambda_1)\cos(1-\lambda_1)\theta\\ (3-\lambda_1)\cos(1-\lambda_1)\theta\\ (1-\lambda_1)\sin(1-\lambda_1)\theta\end{Bmatrix} + \chi_{b_1}(1-\lambda_1)\begin{Bmatrix}\cos(1+\lambda_1)\theta\\ -\cos(1+\lambda_1)\theta\\ \sin(1+\lambda_1)\theta\end{Bmatrix} + \frac{q}{4(q-1)}\left(\frac{r}{r_0}\right)^{\mu_1-\lambda_1}\left(\chi_{d_1}\begin{Bmatrix}(1+\mu_1)\cos(1-\mu_1)\theta\\ (3-\mu_1)\cos(1-\mu_1)\theta\\ (1-\mu_1)\sin(1-\mu_1)\theta\end{Bmatrix} + \chi_{c_1}\begin{Bmatrix}\cos(1+\mu_1)\theta\\ -\cos(1+\mu_1)\theta\\ \sin(1+\mu_1)\theta\end{Bmatrix}\right)\right] \quad (41)$$

It is worth noting that the $\tau_{r\theta}$ stress component is always null along the notch bisector.

Stresses due to mode II loading conditions are

$$\begin{Bmatrix}\sigma_\theta\\ \sigma_r\\ \tau_{r\theta}\end{Bmatrix} = \lambda_2 r^{\lambda_2-1} a_2 \left[\begin{Bmatrix}(1+\lambda_2)\sin(1-\lambda_2)\theta\\ (3-\lambda_2)\sin(1-\lambda_2)\theta\\ (1-\lambda_2)\cos(1-\lambda_2)\theta\end{Bmatrix} + \chi_{b_2}(1+\lambda_2)\begin{Bmatrix}\sin(1+\lambda_2)\theta\\ -\sin(1+\lambda_2)\theta\\ \cos(1+\lambda_2)\theta\end{Bmatrix} + \frac{1}{4(\mu_2-1)}\left(\frac{r}{r_0}\right)^{\mu_2-\lambda_2}\left(\chi_{d_2}\begin{Bmatrix}(1+\mu_2)\sin(1-\mu_2)\theta\\ (3-\mu_2)\sin(1-\mu_2)\theta\\ (1-\mu_2)\cos(1-\mu_2)\theta\end{Bmatrix} + \chi_{c_2}\begin{Bmatrix}-\sin(1+\mu_2)\theta\\ \sin(1+\mu_2)\theta\\ -\cos(1+\mu_2)\theta\end{Bmatrix}\right)\right] \quad (42)$$

Along the notch bisector only the $\tau_{r\theta}$ stress component is different from zero.

For computational convenience, all characteristic parameters present in Eqs. (41) and (42) are given in Tables 1 and 2 as a function of some notch opening angles.

Eqs. (41) and (42) show that the stress components are defined except for constants a_1 and a_2. These constants can be expressed either as a function of a convenient stress value (the stress value at the notch tip, for example, coincident with the peak stress value in the case in which only the mode I stress field is present) or as a function of the notch stress intensity factors (N-SIFs) K_{I} and K_{II}.

Notice that the aim of this formulation is to describe the rounded V-notch stress field in the most highly stressed zones, not the stress distributions in the nominal stress zone. To achieve this task, it is not necessary to take into account for this type of notch the linear combination of multiple solutions concerning several eigenvalues or consider several constants "a_i"; mode I and II notch stress fields are both well described except for a single constant, "a_1" and "a_2, respectively. If, incidentally, the notch degenerates into a corner, the stress distributions have to be considered valid only in the close neighbourhood of the apex, where the

Table 1
Characteristic parameters for mode I loading

2α	λ_1	μ_1	χ_{b1}	χ_{c1}	χ_{d1}
0	0.5	−0.5	1	4	0
π/6	0.5014	−0.4561	1.0707	3.7907	0.0632
π/4	0.5050	−0.4319	1.1656	3.5721	0.0828
π/3	0.5122	−0.4057	1.3123	3.2832	0.0960
π/2	0.5448	−0.3449	1.8414	2.5057	0.1046
2π/3	0.6157	−0.2678	3.0027	1.5150	0.0871
3π/4	0.6736	−0.2198	4.1530	0.9933	0.0673
5π/6	0.7520	−0.1624	6.3617	0.5137	0.0413

Table 2
Characteristic parameters for mode II loading

2α	λ_2	μ_2	χ_{b2}	χ_{c2}	χ_{d2}
0	0.5	−0.5	1	−12	0
$\pi/6$	0.5982	−0.4465	0.9212	−11.3503	−0.3506
$\pi/4$	0.6597	−0.4118	0.8140	−10.1876	−0.4510
$\pi/3$	0.7309	−0.3731	0.6584	−8.3946	−0.4788
$\pi/2$	0.9085	−0.2882	0.2189	−2.9382	−0.2436
$2\pi/3$	1.1489	−0.1980	−0.3139	4.5604	0.5133
$3\pi/4$	1.3021	−0.1514	−0.5695	8.7371	1.1362
$5\pi/6$	1.4858	−0.1034	−0.7869	12.9161	1.9376

first eigenvector dominates. The smaller the opening angle, the smaller is the region of validity (Dunn et al., 1997).

With explicit reference to V-notches with a notch tip radius different from zero, finite element analyses will enable us to define more precisely the degree of accuracy and the range of applicability of the present equations.

3.1. Evaluation of constant a_1

In the presence of a mode I stress field, it is possible to evaluate the relationship between constant a_1 and the maximum stress at the tip. It turns out to be

$$a_1 = \frac{\sigma_{\max}}{\lambda_1 r_0^{\lambda_1 - 1}\left\{1 + \lambda_1 + \chi_{b_1}(1-\lambda_1) + \left[(1+\mu_1)\chi_{d_1} + \chi_{c_1}\right]\{q/4(q-1)\}\right\}} \tag{43}$$

Alternatively, the stress field in the neighbourhood of the notch tip can be expressed as a function of a stress field parameter, mode I N-SIF. Its definition is consistent with the usual SIF definition if the notch radius and opening angle are both null. For a sharp V-shaped notch, Gross and Mendelson (1972) defined such a parameter as follows:

$$K_{\mathrm{I}} = \sqrt{2\pi}\lim_{r\to 0}(\sigma_\theta)_{\theta=0} r^{1-\lambda_1} \tag{44}$$

As is well known, K_{I} governs the stress field not only for $r \to 0$ but in a finite volume surrounding the notch tip. Consider a series of fatigue tests in which the depth of a slim notch is kept constant but the stress concentration factor K_t is varied by modifying the notch root. Experimental data demonstrate that initially the fatigue strength falls rapidly as K_t increases, but beyond the critical value K_t^*, the fatigue limit of the notched specimens remains constant despite decreases of ρ. Smith and Miller (1978) were able to demonstrate that all notches with K_t greater than K_t^* behave identically and can be treated like cracks of the same depth. Under such conditions the choice more convenient is to define K_{I} on the basis of the stress term with exponent λ of Eq. (41). By so doing, the N-SIF for mode I loading turns out to be

$$K_{\mathrm{I}} = \lambda_1\sqrt{2\pi}[1 + \lambda_1 + \chi_{b1}(1-\lambda_1)]a_1 \tag{45}$$

where the constant a_1 has to be determined at a convenient distance from the notch tip, where the stress fields of the rounded and sharp notch practically coincide (Atzori et al., 2001).

Otherwise, by a similar procedure, one might include in the K_{I} definition the term with exponent μ, which contains a higher order singularity. This alternative choice will be discussed in a next note, where some interesting properties of a so-defined generalised N-SIF will be discussed in detail.

Eq. (45) makes it possible to state the relationship present between the maximum stress at the tip and the N-SIF.

$$K_{\mathrm{I}} = \sigma_{\max}\sqrt{2\pi}\left\{ r_0^{1-\lambda_1} \Big/ \left(1 + \frac{(1+\mu_1)\chi_{d_1} + \chi_{c_1}}{(1+\lambda_1) + \chi_{b1}(1-\lambda_1)} \frac{q}{4(q-1)}\right)\right\} \tag{46}$$

Along the bisector, expressions for the two principal stresses are as follows:

$$(\sigma_\theta)_{\theta=0} = \sigma_{\max}\left(\frac{r}{r_0}\right)^{\lambda_1-1} \frac{(1+\lambda_1) + \chi_{b_1}(1-\lambda_1) + \{q/4(q-1)\}(r/r_0)^{\mu_1-\lambda_1}\left[\chi_{d_1}(1+\mu_1) + \chi_{c_1}\right]}{(1+\lambda_1) + \chi_{b_1}(1-\lambda_1) + \{q/4(q-1)\}\left[\chi_{d_1}(1+\mu_1) + \chi_{c_1}\right]} \tag{47}$$

$$(\sigma_r)_{\theta=0} = \sigma_{\max}\left(\frac{r}{r_0}\right)^{\lambda_1-1} \frac{(3-\lambda_1) - \chi_{b_1}(1-\lambda_1) + \frac{q}{4(q-1)}\left(\frac{r}{r_0}\right)^{\mu_1-\lambda_1}\left[\chi_{d_1}(3-\mu_1) - \chi_{c_1}\right]}{(1+\lambda_1) + \chi_{b_1}(1-\lambda_1) + \frac{q}{4(q-1)}\left[\chi_{d_1}(1+\mu_1) + \chi_{c_1}\right]} \tag{48}$$

Often in fatigue life predictions of notched components, only the maximum principal stress component is taken into account. Then Eq. (47) is given here explicitly along the bisector of notches having an opening angle equal to 0°, 45°, 90° and 135°, respectively.

$$2\alpha = 0^\circ \qquad \frac{\sigma_{\max}}{2\sqrt{2}}\rho^{0.5}\left[(x+0.5\rho)^{-0.5} + 0.5\rho(x+0.5\rho)^{-1.5}\right] \tag{49}$$

$$2\alpha = 45^\circ \qquad \frac{\sigma_{\max}}{3.221}\rho^{0.4950}\left[1.0514(x+0.4286\rho)^{-0.4950} + 0.4820\rho^{0.9369}(x+0.4286\rho)^{-1.4319}\right] \tag{50}$$

$$2\alpha = 90^\circ \qquad \frac{\sigma_{\max}}{3.874}\rho^{0.4555}\left[1.2976(x+0.3333\rho)^{-0.4555} + 0.3957\rho^{0.8894}(x+0.333\rho)^{-1.3449}\right] \tag{51}$$

$$2\alpha = 135^\circ \qquad \frac{\sigma_{\max}}{4.940}\rho^{0.3264}\left[2.040(x+0.2\rho)^{-0.3264} + 0.2091\rho^{0.8934}(x+0.2\rho)^{-1.2198}\right] \tag{52}$$

It is worth noting that Eq. (49) coincides with Creager–Paris' equation valid for blunt cracks.

3.2. Evaluation of constant a_2

Since the shear stress is null at the notch tip, it cannot be used to determine constant a_2. A convenient choice is to correlate constant a_2 to mode II N-SIF.

According to Gross and Mendelson definition, mode II N-SIF is

$$K_{\mathrm{II}} = \sqrt{2\pi}\lim_{r\to 0}(\tau_{r\theta})_{\theta=0} r^{1-\lambda_2} \tag{53}$$

Now, by using Eq. (40), such a definition has to upgrade as follows:

$$K_{\mathrm{II}} = -\lambda_2\sqrt{2\pi}[(1-\lambda_2) + \chi_{b_2}(1-\lambda_2)]a_2 \tag{54}$$

4. Accuracy of the new solution

In order to assess the properties and the accuracy of the new equations, it is useful, first of all, to compare results from the formulas obtained with the results of the most important solutions reported in the literature. Like the solution proposed in (Lazzarin and Tovo, 1996), the new solution agrees with the milestones of linear elastic stress analysis of notches, as far as proper geometrical parameters are concerned. When the notch tip radius is equal to zero coefficients c_1, c_2, d_1 and d_2 become zero and the solution agrees with Williams' solution (1952). On the other hand, when the opening angle is equal to zero, only coefficients d_1 and d_2 are equal to zero and the formulas obtained turn out to be exactly the Creager–Paris' solution (1967). Hence when the notch tip radius is also equal to zero, the stress field evaluated is the same given by

the Irwin close to the crack tip (Irwin, 1957) or, more exactly, the same as given by Westergaard (1939), since the so called "T-stress" (parallel to the crack axis) is not present.

The capability of the proposed expression to describe the stress component field has been investigated by comparing the analytical stress distributions with the numerical results obtained by FE analysis of different models. Several notched plates have been considered, including lateral notches and internal "squared" holes; the chosen geometries have been depicted in Fig. 4 and the main geometrical parameters are reported in Table 3. In this first set of conditions, only mode I stress distribution is investigated, taking advantage of the geometry and external loading symmetry.

Due to their nature, Eqs. (41) and (42) are valid only in stress concentration regions and for notches in wide plates, namely in plates where theoretically the width and the notch depth can be regarded as infinite. However, as displayed in Figs. 5 and 6, the accuracy of the equations remains good along the axis of symmetry also for finite width plates, at least until σ_θ stress field intersects the nominal stress line (evaluated on the net area). The smaller the difference between maximum and nominal stress is (i.e. the stress concentration factor K_t), the smaller the range of validity becomes. Since the stress distribution in a relatively large region ahead of a notch tip depends on K_t (Xu et al., 1995), such a range, given in terms of normalized distance $(r - r_0)/\rho$, decreases both with the increasing ρ and with the decreasing notch depth-ligament width ratio.

When the opening angle is equal to or less than 90° (Fig. 5), Eq. (41) give predictions practically coincident with Creager–Paris' solution, due to the small variability of λ_1 from 0° to 90° (Williams, 1952). By increasing the opening angle (Fig. 6), it is evident that the expression for σ_θ is substantially different from Creager–Paris' solution and that it is able to solve the lack of accuracy previously shown in Fig. 3.

By defining now an error index as

$$\Delta\% = \frac{(\sigma_\theta)_{\theta=0,\mathrm{FEM}} - (\sigma_\theta)_{\theta=0,\mathrm{analytical}}}{(\sigma_\theta)_{\theta=0,\mathrm{FEM}}} 100 \tag{55}$$

it is possible to check along the axis of symmetry the accuracy of the proposed formulation at different distances from the notch tip. The results given in Table 4 indicate a considerable overall precision and the independence of the errors from the type of notch. Hence, along the axis of symmetry, the proposed approach is able to deal with notches of different shapes regardless of their opening angle.

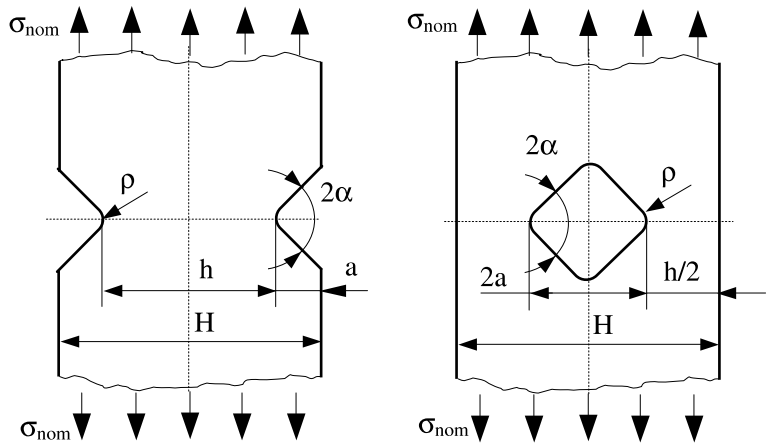

Fig. 4. Models with lateral notches and square holes.

Table 3
Properties of the notches subjected to mode I loading conditions

No.	Type of notch	Notch depth, a (mm)	Opening angle, 2α (°)	Notch tip radius, ρ (mm)	Plate width, H (mm)	Ligament width, h (mm)	$K_{t\,\mathrm{gros}}$	$K_{t\,\mathrm{net}}$
1	Lateral	10	0	2.5	40	20	5.57	2.79
2	Lateral	10	0	2.5	60	40	5.33	3.56
3	Lateral	10	0	1.25	60	40	7.26	4.84
4	Lateral	10	0	0.5	60	40	11.12	7.41
5	Lateral	10	0	0.5	100	80	11.31	9.05
6	Lateral	10	45	2.5	60	40	5.33	3.55
7	Lateral	10	45	1.25	60	40	7.25	4.83
8	Lateral	10	45	0.5	60	40	11.09	7.40
9	Lateral	10	90	2.5	60	40	5.27	3.51
10	Lateral	10	90	1.25	60	40	7.08	4.72
11	Lateral	10	90	0.5	60	40	10.61	7.07
12	Lateral	10	90	0.5	30	10	12.42	4.14
13	Lateral	10	135	2.5	40	20	4.83	2.42
14	Lateral	10	135	2.5	60	40	4.50	3.00
15	Lateral	10	135	2.5	100	80	4.58	3.66
16	Lateral	10	135	0.5	30	10	9.66	3.22
17	Lateral	10	135	0.5	40	20	8.10	4.05
18	Lateral	10	135	0.5	60	40	7.57	5.04
19	Lateral	10	135	0.5	100	80	7.70	6.16
20	Hole	15	0	5	195	165	4.91	4.15
21	Hole	40	0	5	245	165	7.40	4.98
22	Hole	15	45	5	195	165	4.66	3.95

All models present a double symmetry (see Fig. 4).

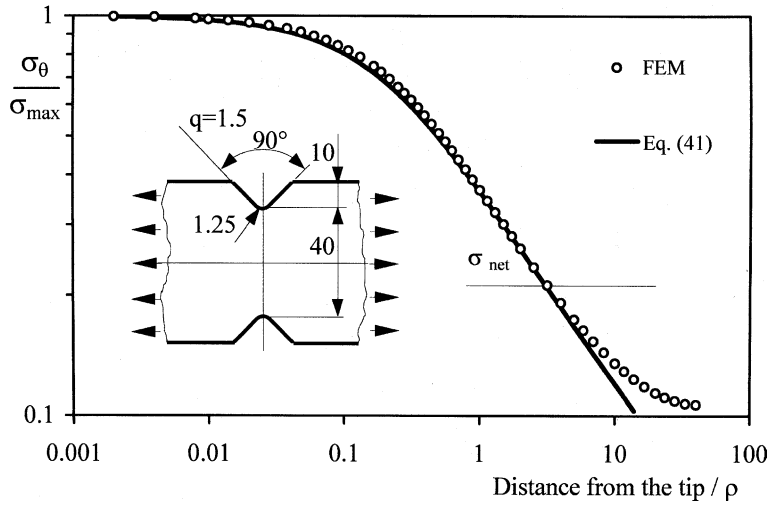

Fig. 5. A comparison between numerical data and analytical predictions (notch no. 10 in Table 1).

Out of the axis of symmetry, it is much more difficult to detail the degree of accuracy of the stress solutions in a finite size plate, since the accuracy depends on the distance from the notch tip, the opening angle, the notch radius and depth and, finally, on the ligament width. However, three models characterised by different values of the opening angle 2α ($2\alpha = 45°$, 90° and 135°, see Fig. 7a–c) enable us to understand the main trends.

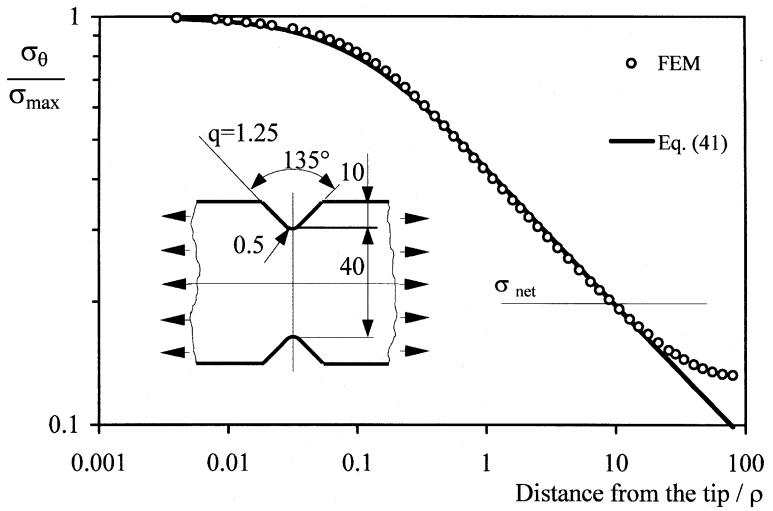

Fig. 6. A comparison between numerical data and analytical predictions (notch no. 18 in Table 1).

Table 4
Error indexes related to the twenty notches considered in Table 3

	[Δ%]							
No. $\frac{r-r_0}{\rho}$	0.1	0.2	0.3	0.4	0.5	0.7	1	3
1	−0.50	−1.27	−1.96	−2.48	−2.76	−2.60	−1.07	(1)
2	−0.90	−2.01	−3.01	−3.82	−4.36	−4.71	−3.84	(1)
3	−0.47	−1.41	−2.41	−3.33	−4.08	−5.12	−5.65	(1)
4	−0.02	−0.76	−1.50	−2.45	−3.32	−4.66	−5.96	−4.80
5	−0.03	−0.77	−1.52	−2.49	−3.37	−4.75	−6.12	−5.47
6	1.07	1.14	0.99	0.76	0.62	1.31	2.00	(1)
7	1.63	1.75	1.53	1.21	0.87	0.42	0.33	(1)
8	1.86	2.31	2.34	1.95	1.51	0.77	0.03	1.97
9	2.66	3.31	3.15	2.85	2.55	2.34	2.72	(1)
10	2.88	3.51	3.38	3.04	2.52	1.81	1.25	(1)
11	3.06	3.90	3.74	3.26	2.74	1.83	0.90	1.34
12	2.94	2.80	2.23	1.86	1.67	1.81	2.7	(1)
13	2.70	2.30	1.43	0.81	0.28	−0.11	−0.06	4.41
14	2.61	2.11	1.11	0.36	−0.32	−0.92	−1.57	0.75
15	2.71	2.31	1.43	0.74	0.202	−0.49	−0.65	0.58
16	2.68	2.23	1.31	0.56	−0.03	−0.71	−1.18	−1.07
17	2.69	2.21	1.26	0.50	0.12	−0.84	−1.40	1.79
18	2.56	4.81	6.32	7.51	8.13	8.21	6.15	(1)
19	1.73	3.59	5.06	6.48	7.49	8.64	9.09	(1)
20	2.13	2.33	2.00	1.15	0.57	−0.42	−1.18	(1)

(1) zone affected by the nominal stress.

These models assure the constancy of the notch depth to notch tip radius ratio ($a/\rho = 20$) as well as the constancy of the ligament width to notch depth ratio ($h/a = 4.0$).

All stress components are normalised with respect to the maximum σ_θ stress component (present at the notch tip) and plotted along a semi-circular arc of which the centre is located at the origin of the (r, θ) coordinate system: the arc intersects the axis of symmetry either at a distance 3ρ from the notch tip (Fig. 7) or at a distance ρ from the notch tip (Fig. 7c).

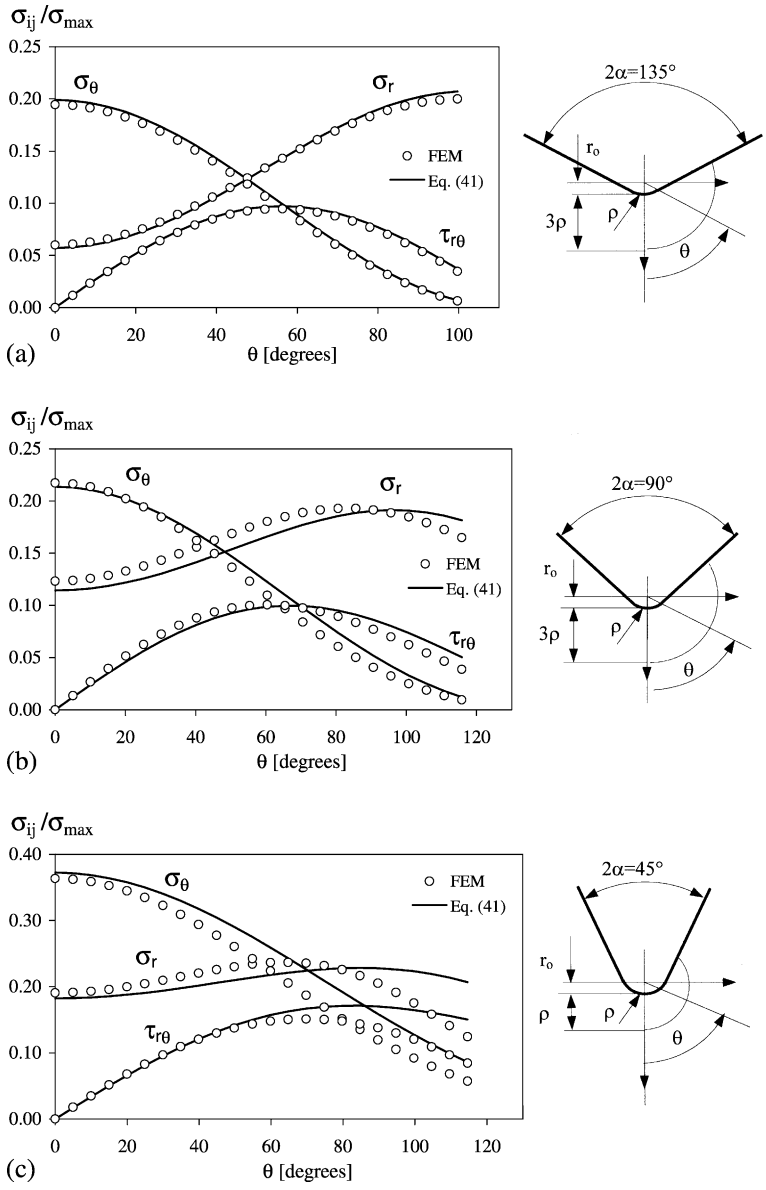

Fig. 7. Stress fields plotted along a circular arc centered on the origin of the (r, θ) system.

In the case with $2\alpha = 135°$ (Fig. 7a, all stress components are in satisfactory agreement with the finite element results along the entire arc of interest, from the notch axis to the notch flank.

The accuracy decreases when the opening angle decreases (Fig. 7b), but it remains very good, at least for the σ_θ stress component despite it being strongly reduced with respect to the maximum value present at the notch tip. An increase of accuracy can be obtained only by reducing the distance from the notch tip. This reduction becomes absolutely necessary for the model with $2\alpha = 45°$ (Fig. 7c), where it is evident that predictions are good for σ_r and $\tau_{r\theta}$ only for $\theta < 60°$ and not in correspondence of the notch flank.

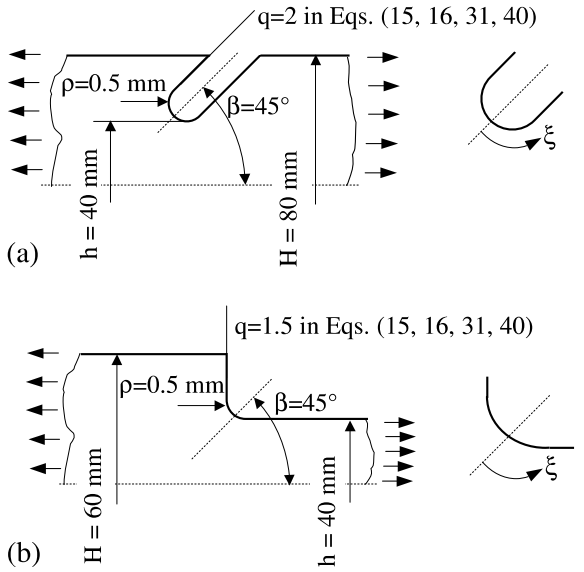

Fig. 8. Shoulder fillet and slanted notches.

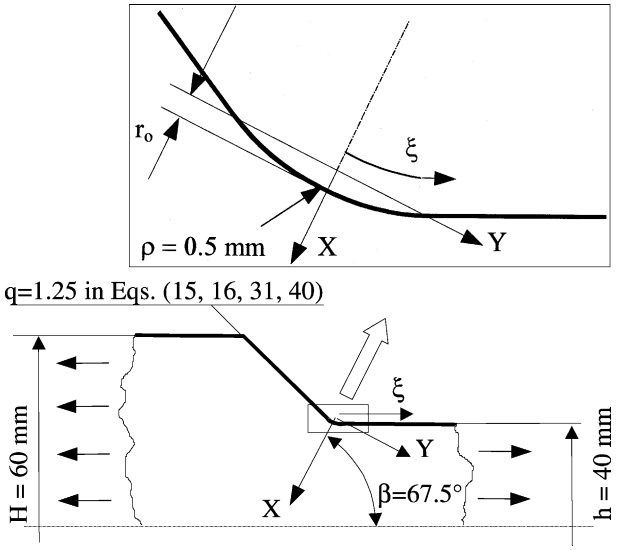

Fig. 9. "Welded-like" geometry.

Further numerical analyses carried out of axis showed that

- the accuracy of the analytical solution tends to increase when the ligament width to notch depth ratio increases, and
- the accuracy decreases when the notch depth to notch tip radius decreases, the minimum value considered by us being $a/\rho = 4.0$.

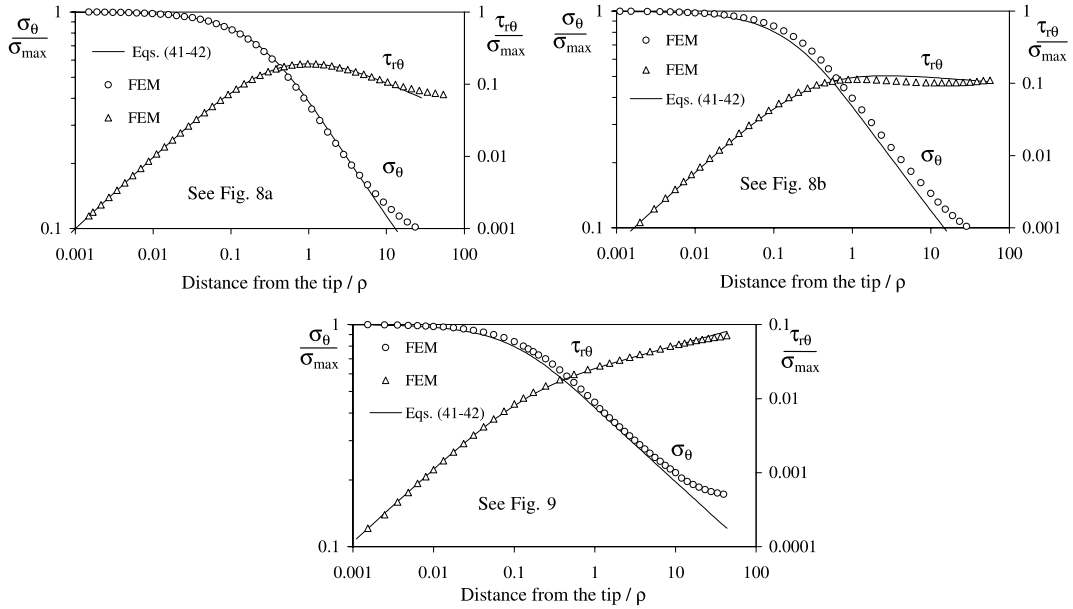

Fig. 10. Stress fields along the bisector of the asymmetric notches shown in Figs. 8 and 9.

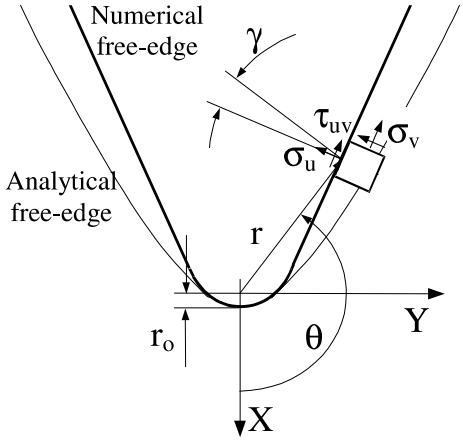

Fig. 11. Local stress parameters along the notch edge.

In order to verify also the accuracy of the mode II solution, the authors think that its investigation alone has no practical application. An effective application field, where modes I and II are present together, is the linear elastic field close to the tip of sloped notches or shoulder fillets. Accurate investigations on sharp V-shaped notches were carried out by Chen (1995) by using the body force method. Even the geometry close to the toe of a weldment can be efficiently investigated as an open notch with a small notch tip radius (Lazzarin and Tovo, 1998) and one of the free edges is usually aligned with the loading direction as well as in the shoulder fillets.

In these geometries, the external-loading direction is not perpendicular to the bisector of the notch and the resulting stress field is the superposition of a mode I (symmetric) and a mode II (skew-symmetric) contributions (Carpenter, 1985). Three reference geometries are considered here: a U-shaped notch slanted

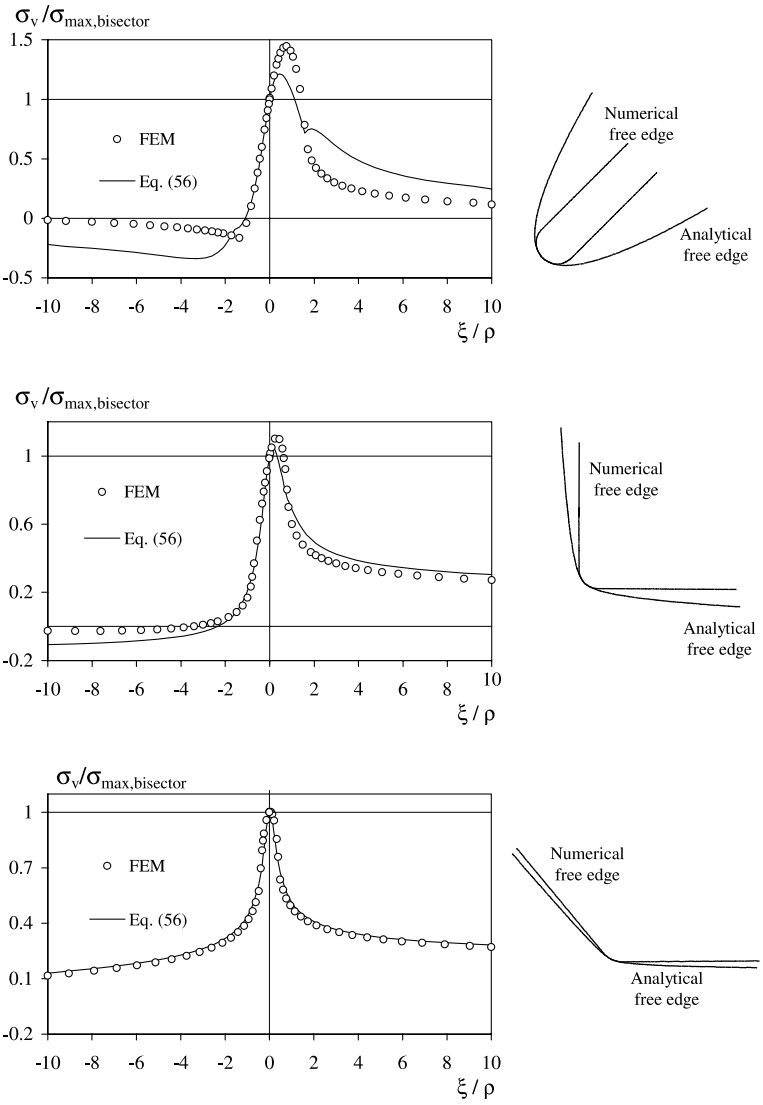

Fig. 12. Stress fields along the free edge of the asymmetric notches.

by 45° with respect to the free edge and the loading direction (Fig. 8a), a shoulder fillet having a opening angle equal to 90° (Fig. 8b) and, finally, a model with a notch with a 135° opening angle, defined as "welded-like" geometry (Fig. 9). In all cases, the gross section and the net section are equal to 60 and 40 mm, respectively. The notch tip radius is equal to 0.5 mm.

When both loading modes are present, their contribution can be separated only along the bisector where σ_θ and σ_r depend on the symmetric mode while $\tau_{r\theta}$ is related to the skew-symmetric mode. The resulting stress fields along the bisector are shown in Fig. 10a–c where theoretical distributions are compared with finite element results. It is clear that the mode I stress field distribution follows the considerations already reported concerning symmetric notches; on the other hand, the improvement given by the new approach in mode II (depicted by the shear stress distribution) accuracy is even more visible.

5. Effect of the approximations on the principal stress along the free edge

Under mixed load conditions, along any direction different from the bisector, the overall stress field should be obtained by combining the two elementary modes. Stresses along the main plate free edge are of particular interest since it is common practice to estimate them by means of direct strain gauge measurements.

In order to properly evaluate the stress field parameters along the notch free edge (where the σ_u and τ_{uv} stresses should be equal to zero), the stress field indexes are translated from the (r,θ) coordinate system to the local (u,v) coordinate system (see Fig. 11). By applying the Cauchy theorem, one obtains

$$\begin{Bmatrix} \sigma_v \\ \sigma_u \\ \tau_{uv} \end{Bmatrix} = [T] \begin{Bmatrix} \sigma_r \\ \sigma_\theta \\ \tau_{r\theta} \end{Bmatrix} \tag{56}$$

where matrix T is as follows:

$$[T] = \begin{bmatrix} \cos^2\gamma & \sin^2\gamma & 2\sin\gamma\cos\gamma \\ \sin^2\gamma & \cos^2\gamma & -2\sin\gamma\cos\gamma \\ -\sin\gamma\cos\gamma & \sin\gamma\cos\gamma & \cos^2\gamma - \sin^2\gamma \end{bmatrix} \tag{57}$$

The principal stress parallel to the free edge (i.e. the σ_v stress component) is plotted in Fig. 12a–c for the three models already shown in Figs. 8 and 9. Such a stress is given versus a curvilinear coordinate ξ having the origin located at the notch tip.

A remarkable difference is evident in the three geometries where the opening angle changes from 0° to 135°. In order to understand the reason for this, it is useful to compare the actual free edge shape used in analytical solutions and in finite element analyses. The profile of the finite element models is made of straight lines and arc of circles. In contrast, the analytical formulation is based on a continuous curve, which corresponds to a parabola in the U-notch case ($2\alpha = 0$) and to a hyperbola-like profile in all the other cases ($2\alpha \neq 0$). As a consequence, the free edge of the numerical models is different from the free edge used in the analytical solution (see Fig. 12a–c). The smaller the opening angle, the greater becomes the difference. When, due to the mode II contribution, the maximum principal stress moves away from the bisector and becomes located in the zone where the arc of cycle is tangent to the straight line, the errors become evident

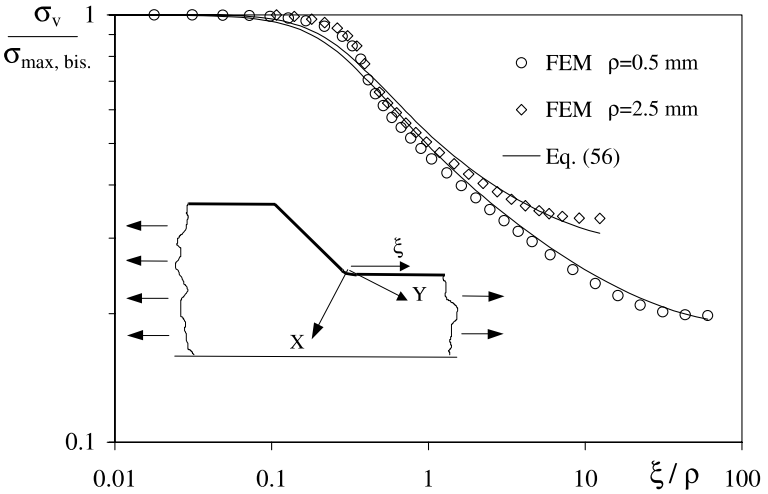

Fig. 13. A comparison along the free edge between numerical data and analytical predictions for two "welded-like" geometry.

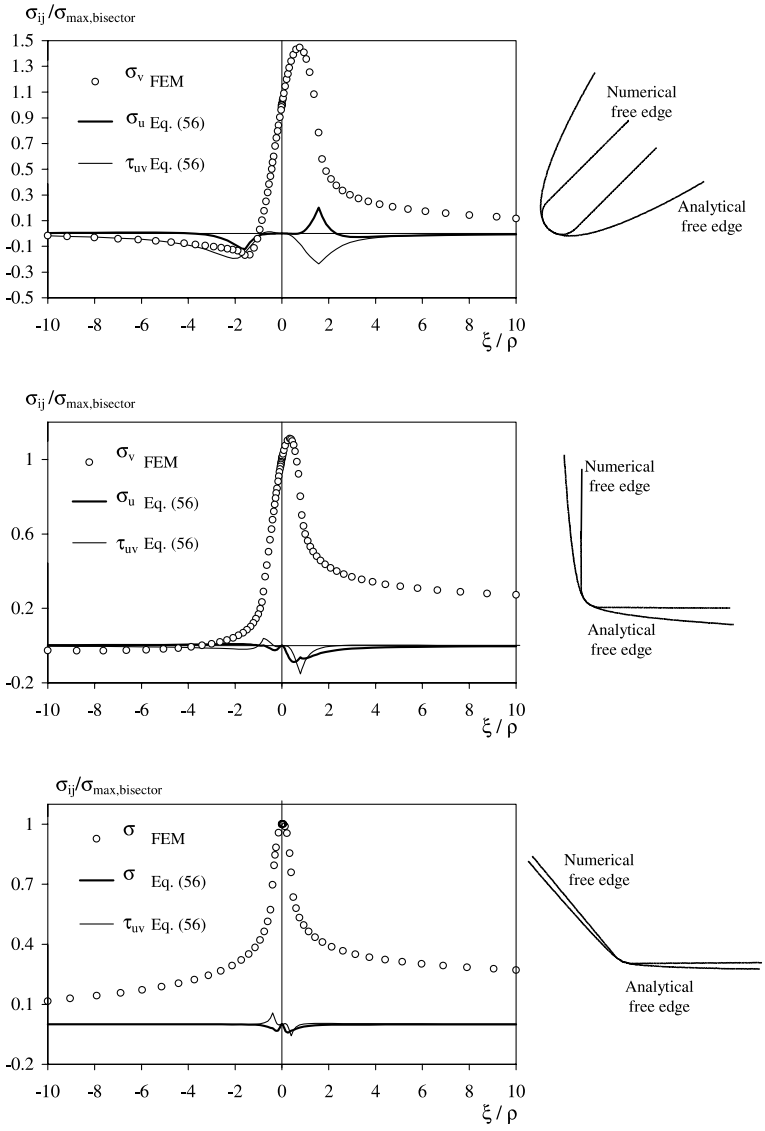

Fig. 14. Stress fields along the free edge of the asymmetric notches.

(Fig. 12a). In the presence of greater opening angles, the agreement is much more satisfactory, in particular in the welded-like geometry.

The greater the opening angle and the distance from the notch tip, the smaller the angle γ and, consequently, the easier the applicability of the boundary conditions provided by Eqs. (8a,b), (21) and (22) to the finite size notches.

To be more precise, a further numerical investigation has also considered a 2.5 mm notch tip radius in the welded-like geometry. The resulting principal stress component, plotted along the main plate free edge by using a double-logarithmic diagram, is shown in Fig. 13. Differences between numerical solution and analytical results are present, once again, in the zone of geometrical transition where the difference between the analytical free edge and the actual free edge is not negligible. However, at distances from the tip

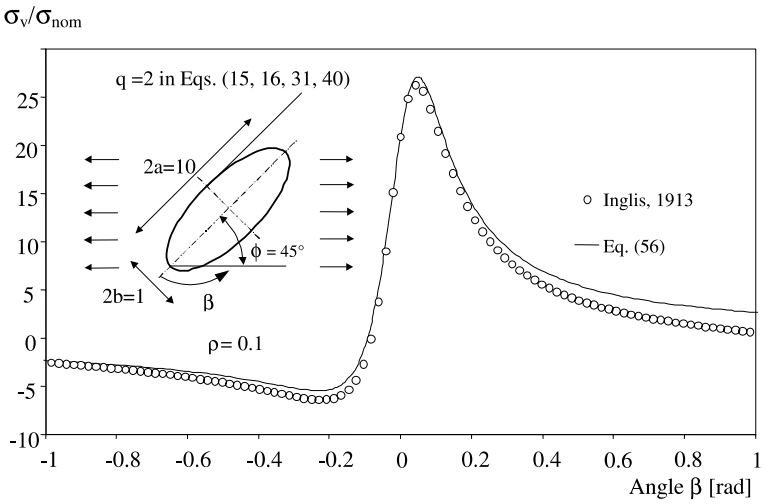

Fig. 15. Stress field along the free edge of an elliptic hole in an infinite plane.

comparable or greater than the notch radius, the agreement is very strong. From a practical point of view, the description of this more distant zone is very useful, because experimental investigations (usually based on strain gauge measurements) are performed at a distance from the tip where the actual weldment geometry is highly affected by welding process irregularities. Therefore, the proposed approach can be used to estimate the whole linear elastic stress field at the weldment toes starting from experimental values determined relatively far away from the notch tip. This theoretical framework shows that the local stress distribution is clearly non linear, as is widely acknowledged, and it is the superposition of a symmetric and skew-symmetric component, so that two parameters must be evaluated for an accurate estimation of the stress field in the neighbourhood of the notch tip. It is important to note that the local stress distribution characterises a reduced zone close to the tip and the zone size can be easily estimated by comparing the free edge stress gradient with respect to the nominal stress value. Therefore experimental measurements along the free edge should take into account whether measured strains (or stresses) are within the local gradient affected zone or not.

Further analyses have considered the stress components σ_u and τ_{uv}. along the free edge. Theoretically these components should be null along the notch free edge: Thus their predicted values give an important information about the accuracy of the approximate solution proposed herein. Fig. 14 plots σ_u and τ_{uv} for the same geometries already shown in Fig. 12. It is evident that the degree of accuracy increases with increasing notch opening angle; likewise for the stress component σ_v.

Finally, the new solution is used to predict the principal stress along the free edge of an ellipse and the approximate results are compared in Fig. 15 with the exact solution provided by Inglis (1913). The ellipse, subjected to mixed load conditions, presents the major axis/minor axis ratio (a/b) equal to 10. When $a/b \geqslant 10$, the new equations are demonstrated to be suitable for providing a satisfactory agreement by setting all parameters with respect to the $2\alpha = 0$ case. This does not hold true when a/b is much smaller than 10.

6. Conclusions

In the present work the problem of the linear elastic stress field close to the tip of V-shaped notches has been addressed. It has been highlighted that several analytical solutions have already been proposed in

literature, but the available solutions are not applicable to notches having a large opening angle and a small notch tip radius. Such a specific problem has already been addressed by the authors, but their previous analytical solution showed a lack of accuracy under particular geometrical circumstances. Hence such a solution has been revised and its accuracy has been strongly improved by adding a component in the polynomial arrangement of potential functions. Consequently, also boundary conditions have been adapted by introducing proper additional conditions.

The result has been an explicit formulation of linear elastic stress components. The formulas have first been compared with Creager–Paris' solution for blunt cracks, as well as with other solutions valid for cracks and sharp corners. Due to the particular choice of the analytical stress functions, it turned out that some widely used equations can be seen as particular cases of the general approach proposed here.

The accuracy of the new solutions was verified by comparing theoretical stress fields and finite element results pertaining to a large set of plane notched models. Non-symmetric geometries were also considered. This comparison is helpful in order to investigate the applicability to cases of engineering interest characterised by the presence of superimposed mode I and II loading conditions.

In the authors' opinion, the overall correctness, as well as the improvement in the accuracy compared to previous closed-form solutions, has been significant.

All equations for mode I and II have been written also by using a commercial code. If requested, the corresponding author (plazzarin@gest.unipd.it) will send the program to all interested readers.

References

Atzori, B., Lazzarin, P., Tovo, R., 1997. Stress distributions for V-shaped notches under tensile and bending loading. Fatigue and Fracture of Engineering Materials and Structures 20, 1083–1092.

Atzori, B., Lazzarin, P., Filippi, S., 2001. Cracks and notches: analogies and differences on the relevant stress distributions and practical consequences in fatigue limit predictions. International Journal of Fatigue 23, 355–362.

Carpenter, W.C., 1984a. A collocation procedure for determining fracture mechanics parameters at a corner. International Journal of Fracture 24, 255–266.

Carpenter, W.C., 1984b. Mode I and mode II stress intensities for plates with cracks of finite opening. International Journal of Fracture 26, 201–214.

Carpenter, W.C., 1985. The eigenvector solution for a general corner or finite opening crack with further studies on the collocation procedure. International Journal of Fracture 27, 63–74.

Chen, D.H., 1995. Stress intensity factors for V-notched strip under tension or in-plane bending. International Journal of Fracture 70, 81–97.

Creager, M., Paris, P.C., 1967. Elastic field equations for blunt cracks with reference to stress corrosion cracking. International Journal of Fracture Mechanics 3, 247–252.

Dunn, M.L., Suwito, W., Cunningham, S., 1997. Fracture initiation at sharp notches: correlation using critical stress intensities. International Journal of Solids and Structures 34, 3873–3883.

Glinka, G., 1985. Calculation of inelastic notch-tip strain-stress hystories under cyclic loading. Engineering Fracture Mechanics 22, 839–854.

Glinka, G., Newport, A., 1987. Universal features of elastic notch-tip stress fields. International Journal of Fatigue 9, 143–150.

Gross, R., Mendelson, A., 1972. Plane elastostatic analysis of V-notched plates. International Journal of Fracture Mechanics 8, 267–276.

Inglis, C.E., 1913. Stresses in a plate due to the presence of cracks and sharp corners. Transactions Institution of Naval Architects 55, 219–230.

Irwin, G.R., 1957. Analysis of stresses and strain near the end of a crack transversing a plate. Journal of Applied Mechanics 24, 361–364.

Kolosov, V., 1909. On the application of complex function theory to plane problem of the mathematical theory of elasticity. Dorpat University.

Kujawski, D., Shin, C.S., 1997. On the elastic longitudinal stress estimation in the neighbourhood of notches. Engineering Fracture Mechanics 56, 137–138.

Lazzarin, P., Tovo, R., 1996. A unified approach to the evaluation of linear elastic fields in the neighbourhood of cracks and notches. International Journal of Fracture 78, 3–19.

Lazzarin, P., Tovo, R., 1998. A notch intensity factor approach to the stress analysis of welds. Fatigue and Fracture of Engineering Materials and Structures 21, 1089–1104.

Lazzarin, P., Tovo, R., Filippi, S., 1998. Stress distribution in finite size plates with edge notches. International Journal of Fracture 91, 269–282.

Muskhelishvili, N.I., 1953. Some basic problems of the mathematical theory of elasticity. Noordhoof Leyden.

Neuber, H., 1958. Theory of Notch Stresses. Springer-Verlag, Berlin.

Smith, R.A., Miller, K.J., 1978. Prediction of fatigue regimes in notched components. International Journal of Mechanical Science 20, 201–206.

Westergaard, H.M., 1939. Bearing pressures and cracks. Journal of Applied Mechanics 6, A49–53.

Williams, M.L., 1952. Stress singularities resulting from various boundary conditions in angular corners of plates in tension. Journal of Applied Mechanics 19, 526–528.

Williams, M.L., 1957. On the stress distribution at the base of a stationary crack. Journal of Applied Mechanics 24, 109–114.

Xu, R.X., Thompson, J.C., Topper, T.H., 1995. Practical stress expressions for stress concentration regions. Fatigue and Fracture of Engineering Materials and Structures 18, 885–895.